IEEE Access
Multidisciplinary | Rapid Review | Open Access Journal

Received 14 January 2024, accepted 10 February 2024, date of publication 13 February 2024, date of current version 23 February 2024.

Digital Object Identifier 10.1109/ACCESS.2024.3365631

RESEARCH ARTICLE

Beamwidth Design Tradeoffs in Radar-Aided Millimeter-Wave Cellular Networks: A Stochastic Geometry Approach

YASSER NABIL[1], HESHAM ELSAWY[2], (Senior Member, IEEE), SUHAIL AL-DHARRAB[3], (Senior Member, IEEE), HASSAN MOSTAFA[4,5], (Senior Member, IEEE), AND HUSSEIN ATTIA[3], (Member, IEEE)

[1]Electrical and Computer Engineering Department, Queen's University, Kingston, ON K7L 3N6, Canada
[2]School of Computing, Queen's University, Kingston, ON K7L 3N6, Canada
[3]Interdisciplinary Research Center for Communication Systems and Sensing, Electrical Engineering Department, King Fahd University of Petroleum and Minerals, Dhahran 31261, Saudi Arabia
[4]Department of Electronics and Communication Engineering, Cairo University, Giza 12613, Egypt
[5]Nanotechnology and Nanoelectronics Program, University of Science and Technology, Zewail City of Science and Technology, Giza 12578, Egypt

Corresponding author: Yasser Nabil (yasser.nabil@queensu.ca)

This work was supported by the King Fahd University of Petroleum and Minerals (KFUPM), Dhahran, Saudi Arabia. Hesham Elsawy was with KFUPM at the start of this work.

ABSTRACT This paper develops a novel stochastic geometry model to investigate design tradeoffs in a large-scale radar-aided millimeter-wave cellular network to eliminate the beam training overhead. In the proposed system, each base station comprises two sub-systems: the sensing sub-system, where radar localizes users, and the communication sub-system, where directional antennas serve the detected users. Both sub-systems operate simultaneously to eliminate the beam training overhead and reduce misalignment errors. The system is modeled under realistic fading conditions with scatterers and interferers in the environment. System parameters, such as the density of mobile users and undesired clutter, radar cross-section fluctuations, radar search duration, antenna directivity, and bandwidth are considered in the analytical model. Two scenarios are studied; the first considers antenna misalignment for the communication sub-system, where error magnitude depends on the radar sub-system accuracy. The other scenario considers perfect alignment for benchmarking. It is demonstrated that the radar search duration, which controls the radar antenna beamwidth, is a crucial parameter for optimizing the system throughput. Moreover, the beamwidth of the communication antenna exhibits a tradeoff in which a narrow beam yields higher gain and reduces interference but increases the misalignment error impact. The results demonstrate that if the beamwidths of both sub-systems are carefully chosen, the proposed system can eradicate the beam training overhead without compromising the system's performance, in addition to significantly enhancing the average total system throughput.

INDEX TERMS Radar-assisted communication, beam training, radar, clutter, radar cross section (RCS), millimeter-wave, beam misalignment error, cellular networks, stochastic geometry.

I. INTRODUCTION

The proliferating bandwidth-hungry applications (e.g., virtual reality, online gaming, and holographic communication) within 5G/6G networks are driving a paradigm shift towards higher frequency bands such as millimeter-wave (mm-wave) and terahertz. To enjoy their enormous bandwidth, high-gain antennas with pencil beams are required to compensate for the significant path loss attenuation at such high frequencies [1], [2]. By virtue of the short wavelengths, it is possible to implement compact-size highly directional antennas with a large number of antenna elements [1], [2].

The associate editor coordinating the review of this manuscript and approving it for publication was Bilal Khawaja.

However, accurate antenna alignment between transmitters (Tx) and receivers (Rx), i.e. beam training, becomes more challenging, where a slight misalignment error can lead to an overwhelming signal attenuation [3], [4], [5], [6]. In general, beam training methods in mm-wave communication can be categorized into three main groups:

- Blind beam training: includes exhaustive search which is the most precise method that tests all possible beam pairs between the Tx and Rx. However, it incurs significant overhead. To reduce this overhead, alternative approaches like hierarchical search and two-stage search are now employed [4].
- Side information-aided beam training: involves gathering information about the user, such as its position, through sensors. This information is utilized to limit the beam search space [3], [4], [5], [6]. These sensors encompass automotive sensors, cameras, or radar-assisted beam training, leveraging information derived from radar to configure mm-wave communication beams.
- Machine learning-based beam training: utilizes information gained from previous training to restrict the search area and predict the next training phase [4].

Nevertheless, blind beam training techniques remain the most widely used in practical systems. These methods are complex and slow due to the substantial number of antenna array elements and the required extensive beam sweeps [3], [4], [5], [6]. A complex and time-consuming beam training process reduces spectrum utilization, which should be better utilized for transmitting user data. A prolonged beam training procedure also has negative consequences on handovers, initial user access, the number of supported users, and total system throughput [3], [4], [5], [6]. This negative impact of beam training is exacerbated with mobility (e.g., vehicular communications), which is more susceptible to beam misalignment errors, and hence, severe connectivity disruptions. In addition, the trained beams rapidly become outdated, necessitating frequent intra-cell and inter-cell handovers [3], [4], [5], [6].

Utilizing the radar sensing capabilities of mm-wave frequencies, beam alignment can be accelerated by estimating the location of mobile users [3], [4], [5], [6], [7], [8], [9], [10]. Owing to the large bandwidth available at the mm-wave band, the precise radar range resolution is plausible, i.e., the ability to detect targets (users) that are close to each other [7], [11]. In such radar-assisted communication systems, the mm-wave communication beams are configured based on the position information obtained from the radar sensing beams. Consequently, this approach alleviates the complexity of estimating real-time channel state information. This can improve the overall system reliability and drastically reduce beam training overhead [3], [4], [5], [6], [7], [8], [9], [10]. For instance, according to [3], obtaining the user position information from the global navigation satellite system (GNSS) can reduce the beam training latency by 53% when compared to the exhaustive search approach. Moreover, authors in [3] show that radar-assisted communication can reduce the beam training latency by 97%.

Although radar-assisted systems can significantly accelerate beam alignment, inaccurate radar detection can result in beam misalignment errors for communication signals; therefore, it is essential to consider the impact of position estimation error in the beamwidth choice [3], [4], [5], [6]. In particular, it is required to balance the gain/error tradeoff in the beamwidth design, where narrower beams exhibit higher gains but are more susceptible to alignment errors, and vice versa [3], [4], [5], [6]. These misalignment errors can significantly impact the performance of mm-wave systems as described in [12]. Consequently, the beamwidth design tradeoff and the effect of potential antenna misalignment errors for the proposed radar-assisted communication systems must be investigated, which is missing in the literature.

A. RELATED WORK

The systems that employ radar for acquiring location information to assist communication in the mm-wave frequency band are studied in [13], [14], [15], [16], and [17]. Particularly, [13] suggests a dual-functional approach to radar communication beamforming, incorporating a power allocation scheme to minimize the overhead associated with beam tracking. In [14], deep learning algorithms trained on location data acquired from radar are employed for beam prediction, leading to a substantial 93% reduction in beam training overhead. In [15] and [16], beam-training overhead is reduced by employing radar to extract the location information, where radar and communication operations are conducted at distinct frequencies. Particularly, [15] demonstrates that theoretically, radar information has the potential to decrease beam training overhead by 97%, although the practical reduction in real-world scenarios may be less than this value. Finally, in [17], the 802.11ad MAC frame is adapted to incorporate radar alongside communication operations, resulting in an 83% reduction in beam training overhead.

All the aforementioned studies leverage radar information to constrain the search space during beam training, thereby reducing overhead. This is necessitated by the presence of localization errors in radar operations, requiring a beam training phase but over a reduced area. In contrast, this paper follows a different approach that eliminates the entire beam training overhead. The radar location information is directly utilized while tolerating associated location errors without requiring additional beam training. In Section V of the results, it is demonstrated that the misalignment error resulting from imperfect radar localization is insignificant when carefully choosing the beamwidths for both radar and communication sub-systems, effectively eliminating the beam training overhead. Moreover, the aforementioned studies merely the performance of single-link or single-cell within a vehicular communication setting. This motivates a large-scale system-level investigation of the beamwidth design tradeoffs in radar-assisted cellular networks.

Stochastic geometry (SG) is a powerful mathematical technique for developing tractable models that analyze random phenomena in the $\mathbb{R}^2$ vector space or higher dimensions [1], [2], [18]. It enables spatial averages, considering vast numbers of nodes at various locations or across multiple spatial realizations. The tractability of SG-based analytical models is a key feature, allowing the extraction of system-design insights that are mainly not achievable through system-level simulations [1], [2], [18]. In a large-scale network setup, SG is indispensable to account for the intrinsically random locations of devices as well as characterizing the mutual interference within the network analytically. In mm-wave networks, SG is widely utilized to account for the impact of directional antennas, as well as the high susceptibility to blockage, on the network performance [1], [2], [18]. In addition, SG is also utilized to study the performance of radar systems [19], [20], [21], [22], [23]. With the growing interest in integrating radar sensing with communication applications; SG tools have recently been applied to assess the performance of such systems as listed in Table 1. However, in all the previous works, the mathematical model lacks either the consideration of clutter effects, radar cross-section (RCS) fluctuations of the target, or a comprehensive analysis of interference. In addition, a perfect alignment is usually assumed for the communication link, which is too idealistic.

B. CONTRIBUTIONS

In this paper, the beamwidth tradeoffs in a mm-wave radar-assisted communication system are studied to eliminate the beam training overhead.[1] A novel mathematical model, based on SG, is developed to evaluate the performance of the proposed system while considering interference from undesirable clutter and the simultaneously transmitting nodes. The numerical results demonstrate the significance of carefully assigning the beamwidths for both radar and communication antennas as crucial design parameters to eliminate beam training overhead without compromising the system's performance as well as enhancing the average total system throughput. The main contributions of this work are:

- In contrast to the previous approaches in the literature that aimed to minimize beam training overhead, the proposed method goes a step further by completely eradicating beam training overhead. This is achieved through the direct utilization of radar information without the need for additional training, tolerating the misalignment error. This error is demonstrated to be insignificant when the beamwidths for both sub-systems are carefully selected.
- To the best of our knowledge, this paper is the first to examine a comprehensive radar-assisted millimeter-wave cellular network on a large-scale level.

[1]This work was partially presented in [34] for an ideal scenario with no consideration of the possible antenna misalignment.

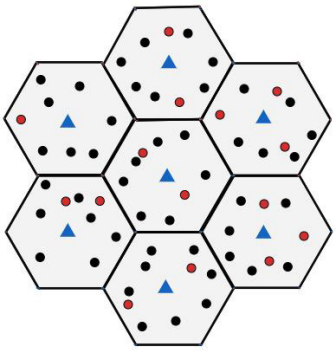

FIGURE 1. The proposed system model (blue triangle: BMR node, red circles: MUs, and black circles: clutter scatterers).

- The proposed analytical model captures the effect of undesirable clutter, RCS fluctuations, and aggregate interference from simultaneously transmitting nodes.
- The effect of antenna misalignment error during communication is considered and evaluated which is missing in previous works.
- The beamwidth design tradeoffs for both the radar and communication sub-systems are characterized.

The remainder of the paper is organized as follows. Section II introduces the system model. Section III presents the radar sub-system analysis that is based on the signal-to-clutter-plus-interference-plus-noise ratio (SCINR). Section IV presents the communication sub-system analysis that is based on the signal-to-interference-plus-noise ratio (SINR). Section V presents the numerical findings and simulations. Finally, Section VI concludes the paper.

II. SYSTEM MODEL

In this section, the system model is described. First, the spatial and transmission models, then the antenna models, and finally, the channel and propagation models.

A. SPATIAL AND TRANSMISSION MODELS

Consider a large-scale network with mobile users (MUs) distributed according to a Poisson Point Process (PPP) ϕ_{MU} with a density of λ_{MU}. The undesirable scatterers whose backscatters represent the clutter (ct) form another PPP ϕ_{ct} as in [21] and [23] with density λ_{ct}. The network area is divided into many adjacent hexagonal small cells of radius R_c. Each cell is equipped with a base station-mounted radar (BMR) node at the cell center, which acts as a monostatic radar, i.e. radar Tx and Rx are co-located, and as a base station (BS) to establish communication links with the detected MUs. These BMR nodes can be supported by the 5G/6G cellular network, and are envisioned as part of future cognitive cities. A depiction of the system model is shown in Figure 1, where the operation of the BMR nodes in different cells is not synchronized. The unambiguous range of a radar R_{max} is the target's maximum range while ensuring that the reflected signal from the target matches the most recent sent pulse such that $R_{max} = \frac{c}{2 f_{PRF}}$, where f_{PRF} is the pulse repetition

TABLE 1. Research works considering SG and integration of radar and communication systems.

Reference	Brief Description	A	B	C	D	E
[24]	Information theoretic analysis for coverage and rate for joint communication and parameter estimation	✗	✓	✓	✓	✗
[25]	A time-division system in which nodes operate as both radars and wireless transmitters	✗	✗	✓	✓	✗
[26]	Radars detect drones using primary beams and share the outcomes through sub-beams	✗	✗	✗	✓	✗
[27]	Radar communication spectrum sharing for collaborative detection in a vehicular network	✗	✗	✓	✓	✗
[28]	Performance of a cellular network that shares spectrum with a rotating radar	✗	✗	✓	✓	✗
[29]	Performance metrics of a time-sharing joint radar communication network	✗	✓	✓	✓	✗
[30]	A collaborative detection leveraging sensing data from multiple BSs to improve object detection	✗	✗	✓	✓	✗
[31]	A time-division system where bistatic radar identifies users to establish communication links with them	✓	✓	✗	✗	✗
[32]	A cellular network with radar operation to boost the resilience of UAV in terms of collision avoidance	✓	✓	✗	✗	✗
[33]	Performance tradeoff in distributed integrated sensing and communication network	✗	✓	✓	✓	✗
This paper	Radar-aided mm-wave cellular network to eliminate the beam training overhead	✓	✓	✓	✓	✓

A: Clutter modeling, B: RCS fluctuations, C: Radar interference, D: Communication interference, E: Misalignment error

frequency (PRF) and c is the speed of light. Accordingly, each node performs a scan of its cell area where $R_{max} = R_c$. Since the departing pulse must physically clear the antenna before the echo can be processed, the minimum range that the radar sub-system can detect is $R_{min} = \frac{c\,\tau}{2}$, where the radar pulse width τ is the reciprocal of the radar bandwidth W_r.

During a fixed search duration, T_r, each BMR node sweeps the azimuthal search space of 2π to cover its cell area. The sensing and communication functionalities are carried out simultaneously at different frequency bands. Therefore, when a MU is detected by the radar sub-system, the communication link is established immediately using a directive beam antenna over a different frequency for a fixed communication time slot duration T_c to avoid any additional delay with detected users. The antenna beam alignment for the communication sub-system is based on the locations detected by the radar sub-system, and hence, misalignment errors are possible for the communication link. The misalignment error angle ϕ is defined between the actual and the detected directions of the MU, which is random but related to radar sub-system accuracy. Moreover, universal frequency reuse is considered, such that the radar band W_r and the communication band W_c are reused in all cells.

Remark 1: The radar and communication sub-systems function simultaneously without interfering with one another since they use different frequency bands. Such simultaneous operation of the two sub-systems highly reduces the impact of misalignment errors during communication. Importantly, the utilization of radar information directly without additional training eliminates beam training overhead, as there is no time wasted on such tasks by the communication sub-system. The cost of eliminating this overhead is the possibility of encountering misalignment errors during communication, which has been demonstrated to be insignificant, as detailed in Section V. Furthermore, the extra bandwidth required for radar is not a major concern within the context of the mm-wave frequency band.

B. ANTENNA MODELS

Consider the half power beamwidth (HPBW) of the Tx and Rx radar sub-system antennas in the azimuthal plane to be θ_{Tx} and θ_{Rx} respectively such that $\theta_{Tx} = \theta_{Rx} = \theta_r$.

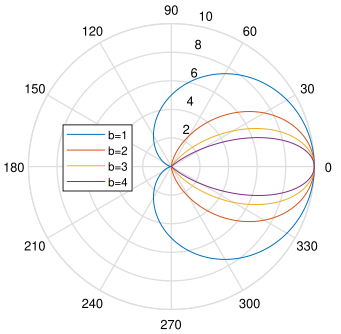

FIGURE 2. Antenna radiation pattern at $G_m = 10$ dBi for different beamwidth spread parameter values.

If a simple parabolic reflector antenna is used, then $\theta_r = \frac{70\lambda}{D}$ [35], where λ is the radar wavelength and D is the antenna diameter. For the radar sub-system, a constant gain and a zero gain are assumed inside and outside the HPBW respectively, where Tx and Rx gains are given by $G_{Tx}(\theta_{Tx}) = G_{Rx}(\theta_{Rx}) = G = \frac{\pi^2 D^2 K_a}{\lambda^2}$ [35], and K_a is the antenna aperture efficiency. Furthermore, let T_b be the antenna beam duration at a fixed direction (dwell time) such that $\frac{2\pi}{\theta_r} = \frac{T_r}{T_b}$, which shows that T_r and θ_r are inversely proportional. For the communication sub-system, the detected MU is assumed to have an omnidirectional antenna while the BMR node communication antenna gain is modeled using the cosine model, which provides a more accurate approximation of the main lobe gains [2] given by

$$G_c(\theta) = \begin{cases} G_m \cos^2\left(\frac{b\theta}{2}\right) & |\theta| \le \frac{\pi}{b} \\ 0 & \text{otherwise} \end{cases} \quad (1)$$

where G_m is the maximum gain, b controls the spread of the antenna beam and θ is the antenna angle relative to the bore sight angle of the antenna. An illustration of the communication sub-system antenna radiation pattern for different values of b is shown in Figure 2.

C. CHANNEL AND PROPAGATION MODELS

Given that both radar and communication sub-systems operate over adjacent frequencies in the same millimeter-wave band. Hence, it is logical to unify the channel conditions assumption for both sub-systems. Owing to the small-cell setup, assume all the MUs within the cell area

have line-of-sight (LOS) conditions as in [2], while the inter-cell interferers can be either in LOS or non-line-of-sight (NLOS) conditions. This assumption aligns with the widely adopted LOS-ball model prevalent in the literature on mm-wave communication [1], [2]. Moreover, from radar's perspective, the assumption of considering only the direct link between radar and target is also widely adopted in mm-wave radar-based systems [19], [20], [21], [22], [23] or joint communication and radar sensing systems [25], [26], [27], [28], [29], [30], [31], [32], [33], [36]. Following [18] and [37], an interference link of length r is in LOS with probability $p_{LOS}(r)$ and NLOS with probability $1 - p_{LOS}(r)$, such that

$$p_{LOS}(r) = e^{-\beta r}, \tag{2}$$

where β is a constant that depends on the geometry and density of the blockage process.

The RCS[2] of the target (the MU in our case) is modeled according to the Swerling I model as in [21], [23], and [33]. In this model, the RCS varies according to a chi-square distribution with two degrees of freedom [38]. This describes the case in which the target velocity is low compared to the observation time and the magnitude of the backscattered signal from the target is relatively constant during T_b [20], [39] which fits our system. On the other hand, the RCS of clutter is modeled using the generalized Weibull distribution as in [21] and [23], which is widely utilized in the literature to model clutter owing to its tractability and adaptability to various environmental conditions [40]. Particularly, here the environment is considered to have clutter whose RCS is comparable to that of the target. In addition, MU, clutter scatterers, and noise statistics are considered fixed during the T_b time but change from one T_b to another, which is acceptable given T_b is in the range of a few milliseconds.

For the communication sub-system and the interfering radar signals, a quasi-static Nakagami-m multipath fading is assumed as in [1] and [2], where the channel gains remain constant during T_c and T_b but randomly change across different intervals. Consequently, channel fading gains are modeled as independent and identically distributed (i.i.d.) Gamma random variables with shape parameters m_L and m_N for LOS and NLOS conditions, respectively.

Remark 2: For tractability in the radar sub-system, the multipath signals from targets are neglected. That is, only the direct reflected signal from a target is considered. This is a plausible approximation owing to the high losses at the mm-wave frequency band and the relatively longer propagation distances of the multi-path radar signals reflected from targets [19], [20], [21], [22], [23].

III. RADAR SUB-SYSTEM ANALYSIS

In this section, The radar sub-system analysis that is based on the SCINR is carried out. First, the SCINR is formulated, then the radar detection probability is derived, and finally, the average radar detection rate is calculated.

[2]RCS is defined as the ratio of the power scattered back to the radar receiver over the incident radar power density per unit of solid angle on the target measured in the far field (i.e., it indicates the target's capacity to reflect radar signals in the direction of the radar).

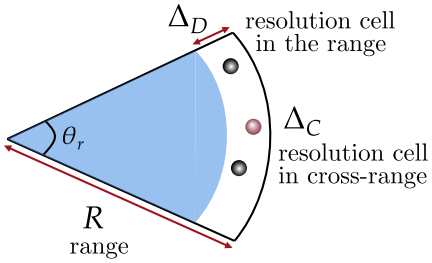

FIGURE 3. Monostatic radar range resolution cell area of $\Delta_D \times \Delta_C$.

A. SCINR FORMULATION

Before formulating the SCINR, the definition of the radar range resolution cell area needs to be introduced. According to [41] and [42], the monostatic radar range resolution cell area is the smallest area in which a radar cannot detect more than one target. It is defined by the size of the resolution cell in the range, $\Delta_D = \frac{c}{2\,W_r}$, and the size of the resolution cell in the cross-range, $\Delta_C = \theta_r R$ as illustrated in Figure 3 then the resolution cell area is

$$A_{rc}(R) = \Delta_D \times \Delta_C = \frac{c\,\theta_r\,R}{2\,W_r}. \tag{3}$$

Without loss of generality, consider a reference BMR node located at the origin. Note that not all the BMR nodes are interfering, but only those BMR nodes whose radar antennas are directed towards the radar antenna of the reference BMR node. As such, the following approximation for the interfering BMR nodes of the radar sub-system is adopted.

Approximation 1: To ensure mathematical tractability and since the BMR nodes density is $\lambda_{\text{BMR nodes}} = \frac{2}{3\sqrt{3}R_c^2}$ but not all BMR nodes are interfering. Accordingly, the actual interfering BMR nodes are approximated by a PPP with density given by

$$\lambda_{I_r} = \frac{2}{3\sqrt{3}R_c^2} \times \frac{\theta_r}{2\pi} \times \frac{\theta_r}{2\pi} \tag{4}$$

where the term $\frac{\theta_r}{2\pi} \times \frac{\theta_r}{2\pi}$ is to capture the probability that the radar antenna of the interfering BMR node is directed towards the radar antenna of the reference BMR node. Moreover, since the nearest BMR node is at distance $2\,R_c$ from the reference node, the interfering BMR nodes are assumed to exist outside an interference-free region, which is approximated via a circle of radius $2\,R_c$ around the origin.

The set of interfering BMR nodes is divided into two independent PPPs for LOS and NLOS conditions. To this end, let Φ_{L_r} be the PPP of LOS interfering BMR nodes with intensity $p_{LOS}(r) \times \lambda_{I_r}$, and Φ_{N_r} be the PPP of NLOS interfering BMR nodes with intensity $(1 - p_{LOS}(r)) \times \lambda_{I_r}$.

As mentioned previously, for a MU at a range of R, the direct signal is only considered and a fixed antenna gain inside the resolution cell is assumed with no returns from the side lobes. For the clutter, only that arises from those

scatterers that are in the same resolution cell as the MU are considered.

According to the radar range equation [42], the signal received from a target, i.e. MU at a range R_{MU}, is given by

$$S(R_{MU}) = \frac{P_r G^2 \sigma_{MU} \lambda^2}{(4\pi)^3 R_{MU}^{2\eta_L} L_s} \tag{5}$$

where P_r is the radar transmitted power, G is the antenna gain, and σ_{MU} is the RCS of the target. Moreover, η_L is the LOS path-loss exponent, and L_s represents system losses, i.e. cable, impedance mismatch, and signal processing loss, among others. The aggregate clutter at the receiver is

$$C = \sum_{ct \in \phi_{ct} \cap A_{rc}(R_{MU})} \frac{P_r G^2 \sigma_{ct} \lambda^2}{(4\pi)^3 R_{ct}^{2\eta_L} L_s} \tag{6}$$

where σ_{ct} is the RCS of the clutter. The thermal noise $N_t = K_B T W_r$, where K_B is Boltzmann constant, and T is the system temperature. The LOS and NLOS interference signals from other cells are given by $I_{L_r} = \sum_{\text{BMR node}_i \in \phi_{L_r}} P_r h_{L_r,i} G^2 C_L r_i^{-\eta_L}$, and $I_{N_r} = \sum_{\text{BMR node}_i \in \phi_{N_r}} P_r h_{N_r,i} G^2 C_N r_i^{-\eta_N}$, where $h_{L_r,i}$ and $h_{N_r,i}$ are the channel gains of the i^{th} LOS and NLOS interfering BMR nodes, respectively, and r_i is the distance between BMR node$_i$ and the origin. C_L and C_N are the LOS and NLOS path-loss intercepts. Therefore, the SCINR for a MU at range R_{MU} is

$$\text{SCINR} = \frac{\frac{P_r G^2 \sigma_{MU} \lambda^2}{(4\pi)^3 R_{MU}^{2\eta_L} L_s}}{\sum_{ct \in \phi_{ct} \cap A_{rc}(R_{MU})} \frac{P_r G^2 \sigma_{ct} \lambda^2}{(4\pi)^3 R_{ct}^{2\eta_L} L_s} + K_B T W_r + I_{L_r} + I_{N_r}}. \tag{7}$$

As the resolution cell area is typically narrow [41], [42], it is plausible to consider that both MU and clutter signals have the same range such that $R_{MU} = R_{ct} = R$ and the SCINR is simplified in (8), as shown at the bottom of the next page.

B. RADAR DETECTION PROBABILITY

To proceed with the analysis, here the radar detection probability is defined as the probability that the average SCINR at range R is greater than or equal to a predefined threshold.[3] This definition was introduced in [21] and [23] but without the interference term. This draws an analogy with coverage probability commonly used in wireless networks, which represents the probability of SINR exceeding a predefined threshold [1], [2]. Additionally, as radar cannot differentiate between multiple MUs within a single resolution cell, it is crucial to account for the probability that the radar resolution cell has only one MU. This probability will be utilized in the subsequent derivation of radar detection probability.

Remark 3: The probability that the radar resolution cell contains a single MU has a zero-truncated Poisson distribution given by

$$\mathbb{P}(\{N(MU) \in A_{rc}(R)\} = 1) = \frac{A_{rc}(R)\, \lambda_{MU}}{e^{A_{rc}(R)\, \lambda_{MU}} - 1} \tag{9}$$

where $N(MU) \in A_{rc}(R)$ denotes the number of MUs in the resolution cell.

Then, the Laplace Transform (LT) of interference is calculated.

Lemma 1: The LT of the aggregate LOS and NLOS interference seen by the typical BMR node located at the origin is given by (10) and (11) respectively.

$$\mathcal{L}_{I_{L_r}}(s) = \exp\left(-2\pi\lambda_{I_r} \int_{2R_c}^{\infty} p_{LOS}(r) \left(1 - \left(1 + \frac{s P_r G^2 C_L r^{-\eta_L}}{m_L}\right)^{-m_L}\right) r\, dr\right) \tag{10}$$

$$\mathcal{L}_{I_{N_r}}(s) = \exp\left(-2\pi\lambda_{I_r} \int_{2R_c}^{\infty} (1 - p_{LOS}(r)) \left(1 - \left(1 + \frac{s P_r G^2 C_N r^{-\eta_N}}{m_N}\right)^{-m_N}\right) r\, dr\right) \tag{11}$$

where $p_{LOS}(r)$ is given by (2).

Proof: See Appendix A. ∎

Utilizing Remark 3 and Lemma 1, the radar detection probability is given in the following theorem.

Theorem 1: The radar detection probability for MU at a range R with a minimum acceptable SCINR threshold γ_r is given in (12), as shown at the bottom of the next page, where σ_{avg_m} is the average RCS of MU, σ_{avg_c} is the average RCS of clutter, and $\mathcal{L}_{I_{L_r}}$, $\mathcal{L}_{I_{N_r}}$ are given by (10) and (11).

Proof: See Appendix B. ∎

C. AVERAGE RADAR DETECTION RATE

The total sweep area by the radar at a range R during the search time duration, T_r, is given by

$$A_{sw} = 2\pi\ R \times \Delta_D = \frac{\pi\ c\ R}{W_r}. \tag{13}$$

Since the spatial distribution of MUs is PPP over the network area, the average number of detected MUs at a range R during one search duration T_r is given by

$$N_d(R) = A_{sw}\ P_d(R)\ \lambda_{MU} = \frac{P_d(R)\ \lambda_{MU}\ \pi\ c\ R}{W_r}, \tag{14}$$

and the average detection rate defined as the average number of detected MUs per second at the range R is given by

$$R_d(R) = \frac{P_d(R)\ \lambda_{MU}\ \pi\ c\ R}{W_r\ T_r}. \tag{15}$$

Remark 4: The range resolution is the ability of the radar to distinguish between targets on the same bearing but at

[3] It is worth mentioning that no assumptions on signal pre-processing before the SCINR computation. The SCINR serves as an initial measure to evaluate the received signal strength in the presence of clutter and interference and to facilitate the theoretical formulation. In practice, a typical target detection system includes various signal processing stages, which is out of the scope of this paper.

different ranges [41]. Hence, theoretically and under ideal conditions, signals reflected from targets on the same bearing can be resolved if the targets are separated by the resolution cell in the range, Δ_D, or more [41]. It is obvious that the number of simultaneously detected targets can be increased by reducing Δ_D through increasing the radar bandwidth.

Utilizing Remark 4, the average total detection rate for any radar sub-system in the network is the sum of the average detection rates at all possible ranges starting from R_{min} to R_c, where each range is separated by Δ_D, to cover the entire search area and is given by

$$R_{dt} = \sum_{i=1}^{\lfloor \frac{2R_c}{c\,\tau} \rfloor} \frac{P_d(\frac{c\,\tau}{2} i)\ \lambda_{MU}\ \pi\ (\frac{c\,\tau}{2} i)\ c}{W_r\ T_r}. \tag{16}$$

IV. COMMUNICATION SUB-SYSTEM ANALYSIS

In this section, the analysis of the communication sub-system based on SINR is performed, then the total system throughput is defined. Without loss of generality, consider a reference detected MU to be located at the origin. The intended link is between the detected MU at the origin and the BMR node at range R where $R \leq R_c$. Furthermore, it is taken into account that the BMR nodes are not transmitting continuously for communication but transmit when a MU is detected by the radar sub-system. As such, the following approximation for the interfering BMR nodes is adopted.

Approximation 2: To ensure mathematical tractability, the interfering BMR nodes are approximated with a PPP of density given by

$$\lambda_{I_c} = \frac{2}{3\sqrt{3}R_c^2} \times\ R_{dt} \times T_c \tag{17}$$

such that $R_{dt} \times T_c \leq 1$, and it captures the probability that an interfering BMR node is active at any time instant. Moreover, due to the absence of intra-cell interference, the interfering BMR nodes are assumed to exist outside an interference-free region, which is approximated via a circle of radius R_c around the typical MU.

The set of interfering BMR nodes is divided into two independent PPPs for LOS and NLOS conditions. To this end, let Φ_{L_c} be the PPP of LOS interfering BMR nodes with intensity $p_{LOS}(r) \times \lambda_{I_c}$, and Φ_{N_c} be the PPP of NLOS interfering BMR nodes with intensity $(1 - p_{LOS}(r)) \times \lambda_{I_c}$. Finally, for the typical detected MU located at the origin and assuming perfect antenna alignment for the intended link, the SINR is given by

$$\text{SINR} = \frac{P_c h_{L,o} G_m C_L R^{-\eta_L}}{I_{L_c} + I_{N_c} + K_B T W_c}, \tag{18}$$

where P_c is the communication sub-system transmission power, $h_{L,o}$ is the intended channel fading gain, and G_m is the maximum antenna gain. The LOS and NLOS interference are given by $I_{L_c} = \sum_{\text{BMR node}_i \in \phi_{L_c}} P_c h_{L,i} G_c(\theta_i) C_L r_i^{-\eta_L}$, and $I_{N_c} = \sum_{\text{BMR node}_i \in \phi_{N_c}} P_c h_{N,i} G_c(\theta_i) C_N r_i^{-\eta_N}$, where $h_{L,i}$ and $h_{N,i}$ are the channel gains of the i^{th} LOS and NLOS interfering BMR nodes, and r_i is the distance between BMR node$_i$ and the origin. Furthermore, θ_i represents the angle formed between the line joining the interferer BMR node$_i$ and its intended MU, and the line joining the interferer BMR node$_i$ with the reference MU positioned at the origin.

A. MISALIGNMENT ERROR

The antenna beam alignment for communication is based on the location of MU detected by the radar sub-system. For an ideal scenario, a perfect beam alignment between the BMR node and detected MU is assumed where $\theta = 0$ and $G_c(\theta) = G_m$. However, since the radar information is employed directly and no further beam training is performed, there exists an error angle ϕ between the actual and the detected directions of the MU as shown in Figure 4. This angle is random but related to the resolution cell in the cross-range, Δ_C. Since only one MU can be detected at any point in the resolution cell with equal probability, the error angle ϕ is modeled as a uniform random variable with a zero mean between $-\frac{\theta_r}{2}$ and $\frac{\theta_r}{2}$, where $|\frac{\theta_r}{2}| < \pi$. It is worth mentioning that a narrower radar beamwidth (i.e., longer search time) leads to decreased misalignment errors in communications due to the reduction in the radar resolution cell area.

The SINR, after considering a misalignment error is

$$\text{SINR} = \frac{P_c h_{L,o} G_c(\phi) C_L R^{-\eta_L}}{I_{L_c} + I_{N_c} + K_B T W_c}. \tag{19}$$

Remark 5: Introducing the misalignment error in the intended link does not affect the interference gain angles, as for each interfering BMR node, θ_i is independent and

$$\text{SCINR}(R) = \frac{\sigma_{MU}}{\sum_{ct \in \phi_{ct} \cap A_{rc}(R)} \sigma_{ct} + \frac{K_B T W_r (4\pi)^3 R^{2\eta_L} L_s}{P_r G^2 \lambda^2} + \frac{I_{L_r} (4\pi)^3 R^{2\eta_L} L_s}{P_r G^2 \lambda^2} + \frac{I_{N_r} (4\pi)^3 R^{2\eta_L} L_s}{P_r G^2 \lambda^2}} \tag{8}$$

$$P_d(R) = \frac{A_{rc}(R)\ \lambda_{MU}}{\exp(A_{rc}(R)\ \lambda_{MU}) - 1} \times \exp\left(\frac{-\gamma K_B T W_r (4\pi)^3 R^{2\eta_L} L_s}{P_r G^2 \lambda^2 \sigma_{avg_m}} + \frac{-\gamma\ \sigma_{avg_c}\ \lambda_{ct}\ c\ \pi\ T_b\ R}{W_r\ T_r\ (\sigma_{avg_m} + \gamma\ \sigma_{avg_c})} \right) \times \mathcal{L}_{I_{L_r}} \left(\frac{\gamma (4\pi)^3 R^{2\eta_L} L_s}{P_r G^2 \lambda^2 \sigma_{avg_m}} \right) \times \mathcal{L}_{I_{N_r}} \left(\frac{\gamma (4\pi)^3 R^{2\eta_L} L_s}{P_r G^2 \lambda^2 \sigma_{avg_m}} \right) \tag{12}$$

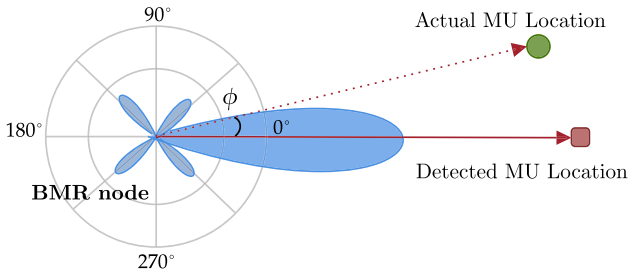

FIGURE 4. Communication antenna misalignment error of angle ϕ between the actual and the detected direction of the MU through radar sub-system.

uniformly distributed. So, after introducing the misalignment error, θ_i distribution remains independent and uniform.

To proceed with the analysis, the probability density function (PDF) of the antenna gain $G(\phi)$ has to be calculated instead of the PDF of ϕ itself.

Lemma 2: The probability distribution of the communication antenna gain with a uniform misalignment error angle $\phi \sim U(-\frac{\theta_r}{2}, \frac{\theta_r}{2})$ is given as follows

$$\mathbb{f}_{G(\phi)}(g(\phi)) = \begin{cases} \dfrac{2}{b\,\theta_r \sqrt{g(\phi)\,(G_m - g(\phi))}} & 0 < g(\phi) < G_m \\ 0 & \text{otherwise} \end{cases} \tag{20}$$

where

$$g(\phi) \in \left[G_m \cos^2\left(\frac{b\,\theta_r}{4}\right), G_m\right] \quad \text{for} \quad \left|\frac{\theta_r}{2}\right| < \frac{\pi}{b}$$
$$g(\phi) \in [0, G_m] \quad \text{for} \quad \frac{\pi}{b} \le \left|\frac{\theta_r}{2}\right| < \pi$$

Proof: Starting with the definition of the cumulative distribution function (CDF) of the gain and performing a transformation of the random variable, i.e.

$$\begin{aligned} &\mathbb{F}_{G(\phi)}(g(\phi)) \\ &= \mathbb{P}\{G(\phi) \le g(\phi)\} \\ &= \mathbb{P}\{-\frac{\theta_r}{2} \le \phi \le -G^{-1}(g(\phi))\} + \mathbb{P}\{G^{-1}(g(\phi)) \le \phi \le \frac{\theta_r}{2}\} \end{aligned} \tag{21}$$

Substituting by the PDF of ϕ and integrating

$$\mathbb{F}_{G(\phi)}(g(\phi)) = \int_{-\frac{\theta_r}{2}}^{-G^{-1}(g(\phi))} \frac{1}{\theta_r}\, d\phi + \int_{G^{-1}(g(\phi))}^{\frac{\theta_r}{2}} \frac{1}{\theta_r}\, d\phi \tag{22}$$

Since $G^{-1}(g(\phi)) = \frac{2}{b}\cos^{-1}\left(\sqrt{\frac{g(\phi)}{G_m}}\right)$, then CDF of gain is

$$\begin{aligned} &\mathbb{F}_{G(\phi)}(g(\phi)) \\ &= 1 - \frac{4}{b\,\theta_r}\cos^{-1}\left(\sqrt{\frac{g(\phi)}{G_m}}\right) \\ &= \begin{cases} 0 & g(\phi) < 0 \\ 1 - \dfrac{2\,\pi}{b\,\theta_r} & g(\phi) = 0 \\ 1 - \dfrac{4}{b\,\theta_r}\cos^{-1}\left(\sqrt{\dfrac{g(\phi)}{G_m}}\right) & 0 < g(\phi) < G_m \\ 1 & g(\phi) \ge G_m \end{cases} \end{aligned} \tag{23}$$

By taking the derivative of the CDF, the lemma is proved. ■

B. COMMUNICATION COVERAGE PROBABILITY

Here the communication coverage probability is calculated for the links established with the detected MUs in the presence of the antenna misalignment error. First, the LT of interference is calculated.

Lemma 3: The LT of the aggregate LOS and NLOS interference seen by the typical MU located at the origin is given by (24) and (25) respectively.

$$\mathcal{L}_{I_{L_c}}(s) = \exp\left(-\lambda_{I_c}\int_{-\frac{\pi}{b}}^{\frac{\pi}{b}}\int_{R_c}^{\infty} p_{LOS}(r) \left(1 - \left(1 + \frac{sP_cG_c(\theta_I)C_L r^{-\eta_L}}{m_L}\right)^{-m_L}\right) r\, dr\, d\theta_I\right) \tag{24}$$

$$\mathcal{L}_{I_{N_c}}(s) = \exp\left(-\lambda_{I_c}\int_{-\frac{\pi}{b}}^{\frac{\pi}{b}}\int_{R_c}^{\infty} (1 - p_{LOS}(r)) \left(1 - \left(1 + \frac{sP_cG_c(\theta_I)C_N r^{-\eta_N}}{m_N}\right)^{-m_N}\right) r\, dr\, d\theta_I\right) \tag{25}$$

where $p_{LOS}(r)$ is given in (2).

Proof: See Appendix C. ■

Utilizing the results of Lemma 2 and Lemma 3, the coverage probability can be derived in the following theorem.

Theorem 2: The communication coverage probability at a range R with a minimum SINR threshold γ_c to correctly decode the signal is given as follows

$$\begin{aligned} &C_p(R) \\ &= \sum_{n=1}^{m_L} (-1)^{n+1}\binom{m_L}{n}\int \exp\left(-\frac{k_L\, n\, \gamma_c\, R^{\eta_L}\, K_B T W_c}{P_{cg_{cC_L}}}\right) \\ &\quad \times \mathcal{L}_{I_{L_c}}\left(\frac{k_L\, n\, \gamma_c\, R^{\eta_L}}{P_{cg_{cC_L}}}\right)\mathcal{L}_{I_{N_c}}\left(\frac{k_L\, n\, \gamma_c\, R^{\eta_L}}{P_{cg_{cC_L}}}\right) f_G(g_c)\, dg_c \end{aligned} \tag{26}$$

where $k_L = m_L(m_L!)^{-\frac{1}{m_L}}$, $\mathcal{L}_{I_{L_c}}$ and $\mathcal{L}_{I_{N_c}}$ are given by (24) and (25).

Proof: See Appendix D. ■

If a perfect antenna alignment is assumed between the detected MU and its BMR node, the coverage probability is given by the following corollary.

Corollary 1: The communication coverage probability in case of perfect antenna alignment between the BMR node and the detected MU is given by

$$C_p(R) = \sum_{n=1}^{m_L} (-1)^{n+1} \binom{m_L}{n} \exp\left(-\frac{k_L\, n\, \theta_t\, R^{\eta_L}\, K_B T W_c}{P_c G_m C_L}\right) \times \mathcal{L}_{I_{L_c}}\left(\frac{k_L\, n\, \theta_t\, R^{\eta_L}}{P_c G_m C_L}\right) \mathcal{L}_{I_{N_c}}\left(\frac{k_L\, n\, \theta_t\, R^{\eta_L}}{P_c G_m C_L}\right) \tag{27}$$

Proof: It is proved similarly to Theorem 2 but the antenna gain of the intended link is deterministic and equals the maximum value G_m. ■

C. SYSTEM THROUGHPUT

The data rate of the communication sub-system can be characterized by its outage capacity, which is

$$C_r(R) = \mathbb{P}\left(SINR > \gamma_c\right) \times \zeta W_c\ \log_2\left(1+\gamma_c\right) \tag{28}$$

where ζ accounts for the gap between the theoretical Shannon capacity and actual modulation and coding schemes. Hence, the average system throughput at distance R corresponds to the product of the average radar detection rate at that distance and the data transmitted by each detected MU within T_c.[4]

$$\mathcal{T}(R) = R_d(R) \times T_c \times C_r(R). \tag{29}$$

While the average total system throughput by any BMR node in bits/s is the sum of the average system throughput at all possible ranges starting from R_{min} to R_c, where each range is separated by Δ_D, to cover the entire search area and is given by

$$\mathcal{T}_t = \sum_{i=1}^{\lfloor \frac{2R_c}{c\,\tau} \rfloor} R_d\left(\frac{c\,\tau}{2} i\right) \times T_c \times C_r\left(\frac{c\,\tau}{2} i\right) \tag{30}$$

Remark 6: The operation of the communication sub-system presented in this section is greatly influenced by the radar sub-system performance as follows:

- The communication antenna misalignment error depends on the radar beam spread (i.e., search time) as presented in Lemma 2.
- The interference in the communication sub-system depends on the total radar detection rate as shown in Approximation 2.
- Since the two sub-systems are working simultaneously, this ensures that the communication sub-system serves the detected MUs without queuing delay, and the localization is as accurate as possible.

[4]The communication sub-system can be extended to serve multiple MUs simultaneously in a single time slot with a single antenna beam using some user grouping techniques such as Non-Orthogonal Multiple Access (NOMA). This is a stand-alone problem that requires power allocation strategy and successive interference cancellation (SIC) mechanism, and hence is left as future work to not dilute the paper's main focus. Employing user grouping techniques will enhance the average total throughput of the system but the core findings regarding eliminating the beam training overhead will remain unchanged.

TABLE 2. Numerical parameters of the proposed system.

Parameter Description	Symbol	Value
System temperature	T	300 K
Radar bandwidth	W_r	150 MHz [21], [23]
Communication bandwidth	W_c	200 MHz
Search time	T_r	0.2 s
Minimum range	R_{min}	1 m
Pulse repetition frequency	f_{PRF}	7.253 MHz
Radar transmission power	P_r	0 dBm [21], [23]
Beam duration	T_b	5 ms
Antenna Aperture efficiency	K_a	0.7
Average RCS of target	σ_{avg_m}	1 m^2 [21], [23]
Clutter density	λ_{ct}	10^5 km^{-2} [21], [23]
Mobile users density	λ_{MU}	10^4 km^{-2}
Average RCS of clutter	σ_{avg_c}	1 m^2 [21], [23]
Total radar system loss	L_s	15 dB
Communication transmission power	P_c	0 dBm
LOS path loss exponent	η_L	2
NLOS path loss exponent	η_N	4
Communication antenna maximum gain	G_m	10 dBi
Beamwidth spread parameter	b	2
LOS Gamma RV shape parameter	m_L	3
NLOS Gamma RV shape parameter	m_N	2
LOS probability constant	β	0.0149 [18]
LOS Path loss intercept	C_L	-61.4 dB [1], [2]
NLOS Path loss intercept	C_N	-72 dB [1], [2]
Communication time-slot	T_c	5 ms
Minimum acceptable SCINR threshold	γ_r	0 dB
Minimum acceptable SINR threshold	γ_c	0 dB
Theoretical-to-practical rate	ζ	0.8

- The average total system throughput in bits/s depends on the total detection rate by the radar sub-system as given in (30).

V. NUMERICAL RESULTS

In this section, numerical demonstrations and simulations are performed. The system is set to operate at the 28 GHz frequency band, which is well-suited for both radar and communication operations and the bandwidths of both sub-systems are non-overlapping. As the majority of current integrated radar and communication applications operate within short range [11], [43], $\lambda_{\text{BMR nodes}} = 900$ BMR nodes/km^2 is selected which corresponds to a network of small cells [44] with radius $R_c = 20.68$ m. The rest of the numerical values of the parameters have been carefully selected to be realistic and are listed in Table 2. It is worth mentioning that the developed mathematical model is valid for a broad range of parameter values, where the selected values in this section are considered to demonstrate the performance results and the effect of antenna misalignment along with the aggregate interference.

Figure 5 compares the analytical expression of the radar detection probability given in Theorem 1 to the simulation of the system with exact node locations for various ranges. The accuracy of the proposed radar sub-system model is validated by the excellent consistency between the derived expression and numerical simulation. The figure also illustrates that the radar detection probability diminishes as the range increases. Figure 6 compares the analytical expressions of the communication coverage probability for the misalignment antenna error scenario given by Theorem 2 and the perfect alignment scenario in Corollary 1 to the simulations of the system with exact node locations at various ranges. Again,

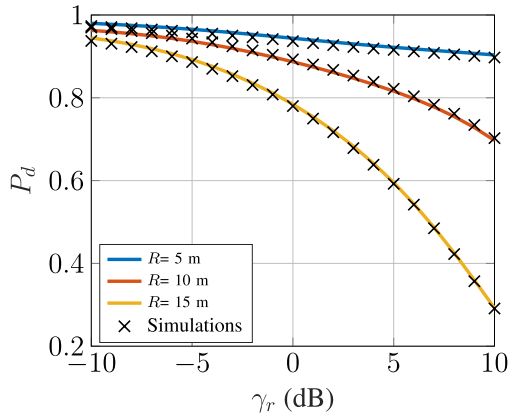

FIGURE 5. Radar detection probability versus the minimum acceptable SCINR threshold for different ranges.

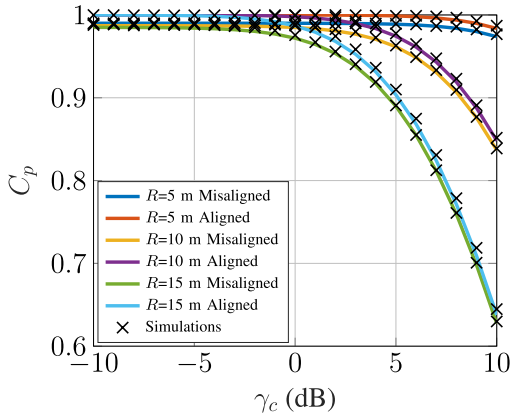

FIGURE 6. Communication coverage probability versus the minimum acceptable SINR threshold for different ranges.

the close match confirms the accuracy of the analytical expressions derived for the communication sub-system. The figure also depicts the deterioration of communication coverage probability due to antenna misalignment.

Figure 7a plots the radar detection probability given by Theorem 1 against the search duration for different ranges. It demonstrates that increasing the search duration increases the radar detection probability. This is due to two factors: increasing search time enables antenna beams to be narrower, thereby enhancing antenna gains. Additionally, narrower beams reduce the area of the resolution cell, which reduces clutter as well as the probability of locating multiple MUs within the same resolution cell. However, after a certain value of T_r, the radar detection probability tends to saturate, as the resolution cell area becomes very small and the system is transformed from clutter-limited to noise-limited operation.

Figure 7b depicts the average radar detection rate calculated in (15) against the search duration. Increasing T_r increases the average radar detection rate due to the improvement in radar detection probability. Nonetheless, there is an optimal T_r above which the average detection rate begins to decline. Beyond the optimal T_r value, the gain in detection due to the increase in radar detection probability becomes insignificant in comparison to the time expended. Figure 8 illustrates that the radar detection probability given by Theorem 1 decreases as the MU density increases due to the increased probability of finding more than one MU in the same resolution cell. Figure 8b shows that the average radar detection rate in (15) increases with increasing MU density because the search area contains more MUs until reaching optimal value. However, a further increase in MU density leads to a decline in the detection rate due to the significant decrease in radar detection probability, as demonstrated in Figure 8.

Figure 9a plots the average radar detection rate in (15) at $R = 15$ m versus MU density for different T_r values while keeping W_r constant. The figure confirms that increasing the search duration in correspondence to the increase in MU density can improve the average radar detection rate. The figure also illustrates that there exists, for each search duration value, an optimal MU density that optimizes the average radar detection rate. Reducing the MU density below this optimal value decreases the density of potential users, thus lowering the average radar detection rate. Increasing MU density above this optimal value decreases the radar detection probability due to the higher probability of locating multiple MUs in one resolution cell. Hence, decreasing the average radar detection rate.

Figure 9b plots the average radar detection rate in (15) at $R = 15$ m versus MU density for different W_r values when T_r is fixed. The figure confirms that increasing the radar bandwidth that reduces the resolution cell area can preserve the average radar detection rate at accepted levels if the MU density is increased. Furthermore, the figure demonstrates that for each radar bandwidth value, there exists an optimal MU density that optimizes the average radar detection rate for the same reasons explained in Figure 9a. However, unlike Figure 9a, this figure shows that the peak of the average radar detection rate always decreases when increasing W_r as a result of amplifying the thermal noise effect.

Figure 10a plots the average total detection rate in (16) versus the search duration at different clutter densities. The figure demonstrates that there exists an optimal search duration that maximizes the average total detection rate. Furthermore, the figure confirms the degradation in performance as clutter density increases. Here for $\lambda_{ct} = 10^5$ km^{-2} and according to the numerical values utilized, the optimal search time duration is approximately 0.16 s which corresponds to radar antenna HPBW of $\theta_r = 11.25°$.

Since introducing the misalignment error transforms the communication antenna gain into a random variable, Figure 10b plots the CDF of the communication antenna gain for $b = 3$ at different radar beamwidth spreads. The figure clearly demonstrates that as the radar beamwidth becomes smaller (i.e., radar search time becomes larger), the probability of having higher communication antenna gain increases. This can be explained as follows: narrower radar beamwidth reduces the radar resolution cell area, which means more accurate radar localization. Consequently, this reduces the misalignment error of the communication

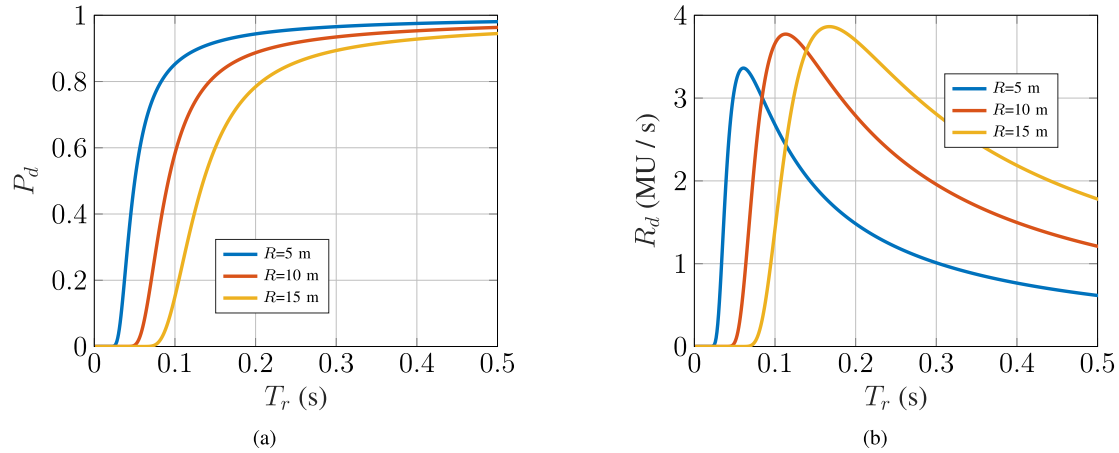

(a) (b)

FIGURE 7. (a) Radar detection probability and (b) Average detection rate versus search duration for different ranges.

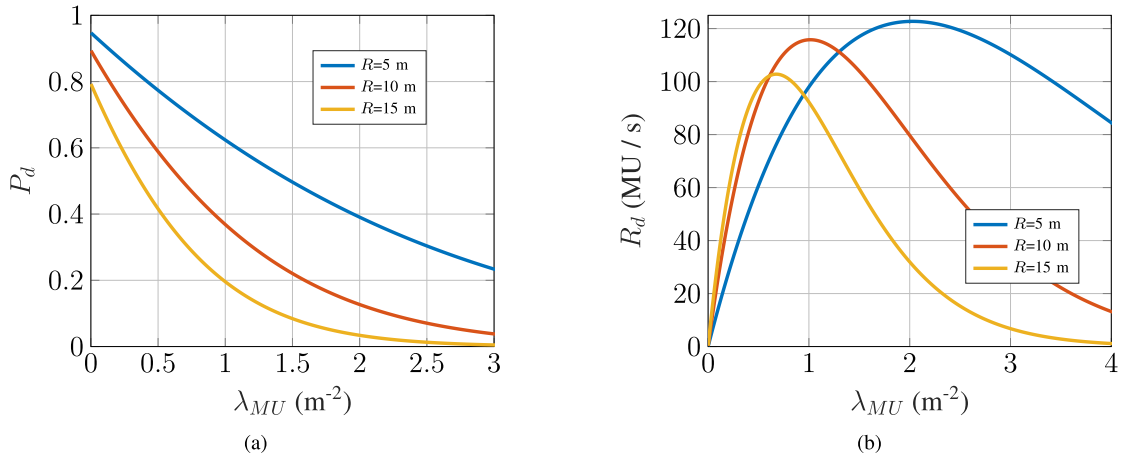

(a) (b)

FIGURE 8. Radar detection probability and average detection rate versus MU density at different ranges.

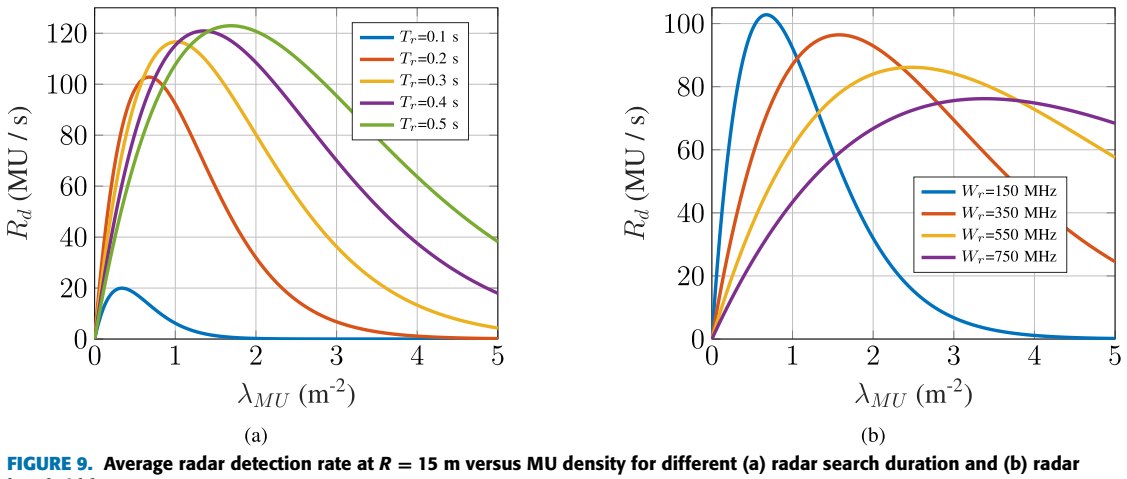

(a) (b)

FIGURE 9. Average radar detection rate at $R = 15$ m versus MU density for different (a) radar search duration and (b) radar bandwidth.

antenna, increasing the probability of having a higher communication antenna gain.

Figure 11 plots the average total system throughput in (30) versus the communication antenna beamwidth spread parameter b at the optimal search duration value that maximizes the radar average total detection rate (i.e., $T_r = 0.16$ s). The results depend on both the communication coverage probability and the radar average detection rate. Moreover, the figure shows that there is an optimal value of b that maximizes the average total system throughput. This can be explained as follows, for the smaller b values corresponding to wide communication antenna beamwidth, the antenna gain

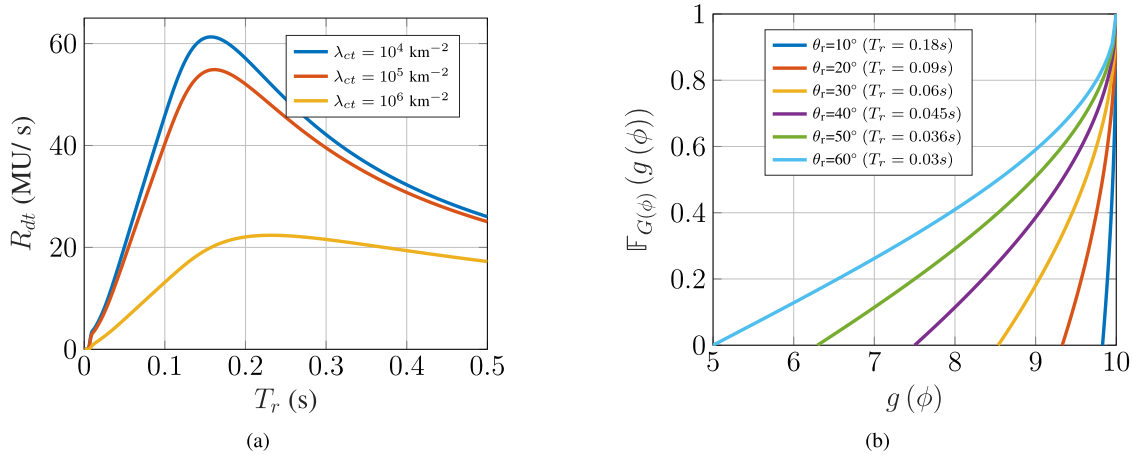

(a) (b)

FIGURE 10. (a) Average total detection rate versus search duration for different clutter densities and (b) CDF of the communication antenna gain at $b = 3$ with misalignment error at different radar HPBW values.

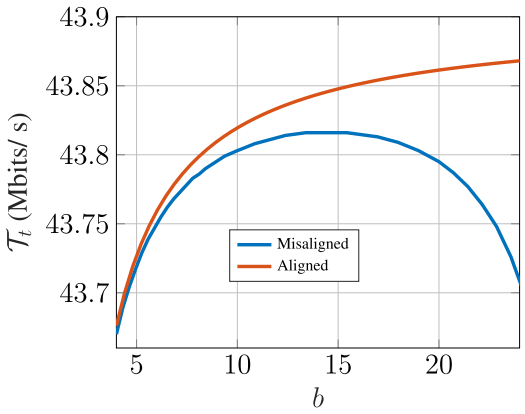

FIGURE 11. Average total throughput versus communication antenna main lobe spread parameter at the optimal search duration value.

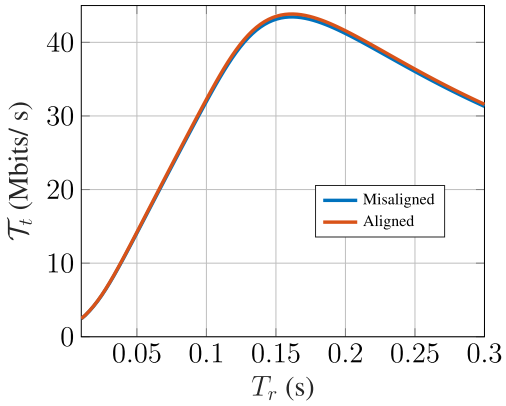

FIGURE 12. Average total throughput versus search duration at the optimal communication antenna main lobe spread parameter.

is small but the penalty of misalignment error is small as well. However, a larger b value, which corresponds to a narrower beamwidth, increases the gain and reduces interference, but the possible misalignment error has a greater impact. On the other hand, if a perfect alignment is considered, increasing b will always enhance the average total system throughput. Here, according to the numerical values utilized, the optimal b is 14.5.

Figure 12 shows the average total system throughput in (30) versus the radar search duration at the optimal communication antenna main lobe spread parameter (i.e., $b = 14.5$). There exists an optimal T_r value that allows for the maximum average total throughput of the system, which is recommended for operation. When employing this optimal value along with the optimal b value, the influence of misalignment error becomes nearly negligible, affirming the effectiveness of the proposed system in eliminating beam training overhead without compromising system performance. Additionally, the observed trends in the figure mirror those in Figure 10a. This consistency is noteworthy as it indicates that the radar sub-system's performance dominates the entire system when an optimal communication antenna beam spread is employed.

VI. CONCLUSION AND FUTURE WORK

This paper introduces an SG model for a radar-assisted communication system operating in the mm-wave band, aiming to eliminate beam training overhead. The model takes into account clutter, RCS fluctuations, and interference from concurrently transmitting nodes. The system comprises two sub-systems: a sensing radar sub-system for locating MUs and a communication sub-system to establish links with detected MUs. Both sub-systems operate simultaneously under realistic LOS and NLOS conditions. To eradicate beam training overhead, the communication antenna's beam alignment relies on the detected MUs' locations from the radar sub-system without additional training. Consequently, a misalignment error is present, and its magnitude is related to the radar sub-system's accuracy.

The results indicate that the proposed system successfully eliminates beam training overhead without compromising system performance. Additionally, the findings highlight that the radar's sub-system dominates the overall system performance when the communication sub-system adopts a suitable antenna beamwidth. Specifically, the communication antenna's beamwidth has a tradeoff, where a narrow

beamwidth provides higher gain, and significantly reduces interference, but amplifies the effects of misalignment error. In summary, two key design parameters crucially impact overall system performance: the radar search duration, influencing radar antenna beamwidth and resolution cell size, and the communication antenna beamwidth which involves a tradeoff. Optimal values for these parameters can greatly enhance the system's average total throughput and effectively eliminate beam training overhead.

While this paper showcased the viability of eliminating beam training overhead in mm-wave communication through the utilization of radar location information and controlling the beamwidth tradeoff, there exists potential for further enhancements. As a future extension of this research, an opportunity lies in addressing the open research challenge related to radar detection in environments marked by NLOS conditions or the presence of shadowing effects. Additionally, the exploration of user grouping techniques, such as NOMA, to simultaneously serve multiple MUs within the same time slot could be considered to enhance the system's throughput.

APPENDIX A
PROOF OF LEMMA 1

Starting with the LOS interference and using the definition of Laplace Transform

$$\begin{aligned}
&\mathcal{L}_{I_{L_r}}(s)\\
&= \mathbb{E}_{\phi_{L_r}}\left[\exp\left(-sI_{L_r}\right)\right]\\
&= \mathbb{E}_{\phi_{L_r}}\left[\exp\left(-s\sum_{\text{BMR node}_i\in\phi_{L_r}} P_r h_{L_r,i} G^2 C_L r_i^{-\eta_L}\right)\right]\\
&= \mathbb{E}_{\phi_{L_r}}\left[\prod_{\text{BMR node}_i\in\phi_{L_r}} \exp\left(-sP_r h_{L_r,i} G^2 C_L r_i^{-\eta_L}\right)\right]
\end{aligned} \tag{31}$$

From the Gamma distribution's moment-generating function

$$\mathcal{L}_{I_{L_r}}(s) = \mathbb{E}_{\phi_{L_r}}\left[\prod_{\text{BMR node}_i\in\phi_{L_r}} \left(1+\frac{sP_r G^2 C_L r_i^{-\eta_L}}{m_L}\right)^{-m_L}\right] \tag{32}$$

Using polar coordinates and the definition of probability generating functional (PGFL) in PPP

$$\mathcal{L}_{I_{L_r}}(s) = \exp\left(-2\pi\lambda_{I_r}\int_{2R_c}^{\infty} p_{LOS}(r) \left(1-\left(1+\frac{sP_r G^2 C_L r^{-\eta_L}}{m_L}\right)^{-m_L}\right) r\, dr\right) \tag{33}$$

where r is the distance from the origin to the interfering BMR node.

For NLOS interference, the previous steps are repeated, replacing $p_{LOS}(r)$ by $(1-p_{LOS}(r))$, m_L by m_N, C_L by C_N and η_L by η_N.

APPENDIX B
PROOF OF THEOREM 1

Let γ be the minimum acceptable SCINR threshold, then the radar detection probability at range R given a single MU exists in the resolution cell is

$$\begin{aligned}
&P_d(R|N(MU)\in A_{rc}(R)=1)\\
&= \mathbb{P}(SCINR>\gamma)\\
&= \mathbb{P}\left[\sigma_{MU} > \frac{\gamma K_B T W_r (4\pi)^3 R^{2\eta_L} L_s}{P_r G^2\lambda^2} + \frac{\gamma I_{L_r}(4\pi)^3 R^{2\eta_L} L_s}{P_r G^2\lambda^2}\right.\\
&\quad \left. + \frac{\gamma I_{N_r}(4\pi)^3 R^{2\eta_L} L_s}{P_r G^2\lambda^2} + \sum_{ct\in\phi_{ct}\cap A_{rc}(R)} \gamma\ \sigma_{ct}\right]
\end{aligned} \tag{34}$$

Adopting the Swerling I model, the PDF of σ_{MU} reduces to

$$\mathbb{P}(\sigma_{MU}) = \frac{1}{\sigma_{avg_m}}\exp\left(\frac{-\sigma_{MU}}{\sigma_{avg_m}}\right) \tag{35}$$

which is exponential distribution with mean σ_{avg_m} denoting the average RCS of MU. Then (34) can be written as

$$\begin{aligned}
&P_d(R|N(MU)\in A_{rc}(R)=1)\\
&= \exp\left(\sum_{ct\in\phi_{ct}\cap A_{rc}(R)} \frac{-\gamma\sigma_{ct}}{\sigma_{avg_m}}\right.\\
&\quad \left. - \frac{\gamma(4\pi)^3 R^{2\eta_L} L_s (K_B T W_r + I_{L_r} + I_{N_r})}{P_r G^2\lambda^2\sigma_{avg_m}}\right)\\
&= \exp\left(\frac{-\gamma K_B T W_r (4\pi)^3 R^{2\eta_L} L_s}{P_r G^2\lambda^2\sigma_{avg_m}}\right) \times \mathcal{L}_{I_{L_r}}\left(\frac{\gamma(4\pi)^3 R^{2\eta_L} L_s}{P_r G^2\lambda^2\sigma_{avg_m}}\right)\\
&\quad \times \mathcal{L}_{I_{N_r}}\left(\frac{\gamma(4\pi)^3 R^{2\eta_L} L_s}{P_r G^2\lambda^2\sigma_{avg_m}}\right)\\
&\quad \times \mathbb{E}_{ct,\sigma_{ct}}\left[\exp\left(\sum_{ct\in\phi_{ct}\cap A_{rc}(R)} \frac{-\gamma\sigma_{ct}}{\sigma_{avg_m}}\right)\right]
\end{aligned} \tag{36}$$

Let

$$\begin{aligned}
A &= \mathbb{E}_{ct,\sigma_{ct}}\left[\exp\left(\sum_{ct\in\phi_{ct}\cap A_{rc}(R)} \frac{-\gamma\sigma_{ct}}{\sigma_{avg_m}}\right)\right]\\
&= \mathbb{E}_{ct}\left[\prod_{ct\in\phi_{ct}\cap A_{rc}(R)} \mathbb{E}_{\sigma_{ct}}\left[\exp\left(\frac{-\gamma\sigma_{ct}}{\sigma_{avg_m}}\right)\right]\right].
\end{aligned} \tag{37}$$

Using the PGFL of PPP

$$A = \exp\left(-\lambda_{ct}\iint_{A_{rc}(R)} \mathbb{E}_{\sigma_{ct}}\left[1-\exp\left(\frac{-\gamma\sigma_{ct}}{\sigma_{avg_m}}\right)\right] dx\, dy\right) \tag{38}$$

Substituting by the area of resolution cell and calculating the expectation

$$\begin{aligned}
&A\\
&= \exp\left(-\frac{\lambda_{ct} P\ c\ \theta_r\ R}{2\ W_r}\int_0^{\infty}\left(1-\exp\left(\frac{-\gamma\sigma_{ct}}{\sigma_{avg_m}}\right)\right)\mathbb{P}(\sigma_{ct})\, d_{\sigma_{ct}}\right)
\end{aligned} \tag{39}$$

The Weibull PDF of RCS of clutter at radar, σ_{ct}, is given by

$$\mathbb{P}(\sigma_{ct}) = \frac{k}{\sigma_{avg_c}} \left(\frac{\sigma_{ct}}{\sigma_{avg_c}}\right)^{k-1} \exp\left(-\left(\frac{\sigma_{ct}}{\sigma_{avg_c}}\right)^{k}\right) \quad (40)$$

where σ_{avg_c} is the average RCS of clutter, and k is the shape parameter whose value can capture different conditions.

For the case where clutter arises from discrete scatterers whose RCSs are comparable to that of the target, $k = 1$ is considered as in [21] and [23]. Consequently, the distribution is reduced to exponential which is widely accepted in the literature, and then A in (39) can be simplified to

$$A = \exp\left(\frac{-\gamma\ \sigma_{avg_c}\ \lambda_{ct}\ c\ \theta_r\ R}{2\ W_r\ \left(\sigma_{avg_m} + \gamma\ \sigma_{avg_c}\right)}\right). \quad (41)$$

By utilizing the probability distribution of $(N(MU) \in A_{rc}(R) = 1)$ described in Remark 3, the theorem is proved.

APPENDIX C
PROOF OF LEMMA 3

Starting with the LOS interference, using the definition of Laplace Transform

$$\begin{aligned}
&\mathcal{L}_{I_{L_c}}(s) \\
&= \mathbb{E}_{\phi_{L_c}}\left[\exp\left(-sI_{L_c}\right)\right] \\
&= \mathbb{E}_{\phi_{L_c}}\left[\exp\left(-s \sum_{\text{BMR node}_i \in \phi_{L_c}} P_c h_{L,i} G_{c_i}(\theta_I) C_L r_i^{-\eta_L}\right)\right] \\
&= \mathbb{E}_{\phi_{L_c}}\left[\prod_{\text{BMR node}_i \in \phi_{L_c}} \exp\left(-sP_c h_{L,i} G_{c_i}(\theta_I) C_L r_i^{-\eta_L}\right)\right]
\end{aligned} \quad (42)$$

From the Gamma distribution's moment-generating function

$$\begin{aligned}
&\mathcal{L}_{I_{L_c}}(s) \\
&= \mathbb{E}_{\phi_{L_c}}\left[\prod_{\text{BMR node}_i \in \phi_{L_c}} \left(1 + \frac{sP_c G_{c_i}(\theta_I) C_L r_i^{-\eta_L}}{m_L}\right)^{-m_L}\right]
\end{aligned} \quad (43)$$

Combining BMR nodes' location with their orientations and from the definition of PGFL in PPP

$$\begin{aligned}
\mathcal{L}_{I_{L_c}}(s) = \exp\Bigg(-\lambda_{I_c} \int_{-\frac{\pi}{b}}^{\frac{\pi}{b}} \int_{R_c}^{\infty} p_{LOS}(r) \\
\left(1 - \left(1 + \frac{sP_c G_c(\theta_I) C_L r^{-\eta_L}}{m_L}\right)^{-m_L}\right) r\ dr\ d\theta_I\Bigg)
\end{aligned} \quad (44)$$

where r is the distance from the origin to the interfering BMR node.

For NLOS interference, the previous steps are repeated, replacing $p_{LOS}(r)$ by $(1 - p_{LOS}(r))$, m_L by m_N, C_L by C_N and η_L by η_N.

APPENDIX D
PROOF OF THEOREM 2

Let θ_t be the SINR threshold required to correctly decode the signal, then

$$\begin{aligned}
&C_p(R) \\
&= \mathbb{P}\left(SINR > \theta_t\right) = \mathbb{P}\left(\frac{P_c h_{L,o} G_c(\phi) C_L R^{-\eta_L}}{I_{L_c} + I_{N_c} + K_B T W_c} > \theta_t\right) \\
&= \mathbb{P}\left(h_{L,0} > \theta_t R^{\eta_L} \left(P_c G_c(\phi) C_L\right)^{-1} \times \left(I_{L_c} + I_{N_c} + K_B T W_c\right)\right)
\end{aligned} \quad (45)$$

Utilizing Alzer's inequality [45]

$$\begin{aligned}
C_p(R) \approx \sum_{n=1}^{m_L} (-1)^{n+1} \binom{m_L}{n} \\
\times \mathbb{E}\left[\exp\left(-\frac{k_L\ n\ \theta_t\ R^{\eta_L}\ \left(I_{L_c} + I_{N_c} + K_B T W_c\right)}{P_c G_c(\phi) C_L}\right)\right]
\end{aligned} \quad (46)$$

where $k_L = m_L (m_L!)^{-\frac{1}{m_L}}$

since ϕ_L and ϕ_N are independent and from the definition of Laplace Transform

$$\begin{aligned}
C_p(R) = \sum_{n=1}^{m_L} (-1)^{n+1} \binom{m_L}{n} \exp\left(-\frac{k_L\ n\ \theta_t\ R^{\eta_L}\ K_B T W_c}{P_c G_c(\phi) C_L}\right) \\
\times \mathcal{L}_{I_{L_c}}\left(\frac{k_L\ n\ \theta_t\ R^{\eta_L}}{P_c G_c(\phi) C_L}\right) \mathcal{L}_{I_{N_c}}\left(\frac{k_L\ n\ \theta_t\ R^{\eta_L}}{P_c G_c(\phi) C_L}\right)
\end{aligned} \quad (47)$$

since $G_c(\phi)$ is a random parameter, let $G_c(\phi) = g_c$ with distribution $f_G(g_c)$ then $C_p(R)$ will be given by

$$\begin{aligned}
&C_p(R) \\
&= \sum_{n=1}^{m_L} (-1)^{n+1} \binom{m_L}{n} \int \exp\left(-\frac{k_L\ n\ \theta_t\ R^{\eta_L}\ K_B T W_c}{P_c g_c C_L}\right) \\
&\times \mathcal{L}_{I_{L_c}}\left(\frac{k_L\ n\ \theta_t\ R^{\eta_L}}{P_c g_c C_L}\right) \mathcal{L}_{I_{N_c}}\left(\frac{k_L\ n\ \theta_t\ R^{\eta_L}}{P_c g_c C_L}\right) f_G(g_c)\, dg_c.
\end{aligned} \quad (48)$$

REFERENCES

[1] J. G. Andrews, T. Bai, M. N. Kulkarni, A. Alkhateeb, A. K. Gupta, and R. W. Heath, "Modeling and analyzing millimeter wave cellular systems," *IEEE Trans. Commun.*, vol. 65, no. 1, pp. 403–430, Jan. 2017.

[2] X. Yu, J. Zhang, M. Haenggi, and K. B. Letaief, "Coverage analysis for millimeter wave networks: The impact of directional antenna arrays," *IEEE J. Sel. Areas Commun.*, vol. 35, no. 7, pp. 1498–1512, Jul. 2017.

[3] A. Ali, N. Gonzalez-Prelcic, R. W. Heath Jr., and A. Ghosh, "Leveraging sensing at the infrastructure for mmWave communication," *IEEE Commun. Mag.*, vol. 58, no. 7, pp. 84–89, Jul. 2020.

[4] Y. Wang, Z. Wei, and Z. Feng, "Beam training and tracking in mmWave communication: A survey," 2022, *arXiv:2205.10169*.

[5] N. Gonzalez-Prelcic, A. Ali, V. Va, and R. W. Heath, "Millimeter-wave communication with out-of-band information," *IEEE Commun. Mag.*, vol. 55, no. 12, pp. 140–146, Dec. 2017.

[6] J. Choi, V. Va, N. Gonzalez-Prelcic, R. Daniels, C. R. Bhat, and R. W. Heath, "Millimeter-wave vehicular communication to support massive automotive sensing," *IEEE Commun. Mag.*, vol. 54, no. 12, pp. 160–167, Dec. 2016.

[7] F. Liu, Y. Cui, C. Masouros, J. Xu, T. X. Han, Y. C. Eldar, and S. Buzzi, "Integrated sensing and communications: Toward dual-functional wireless networks for 6G and beyond," *IEEE J. Sel. Areas Commun.*, vol. 40, no. 6, pp. 1728–1767, Jun. 2022.
[8] A. Liu, Z. Huang, M. Li, Y. Wan, W. Li, T. X. Han, C. Liu, R. Du, D. K. P. Tan, J. Lu, Y. Shen, F. Colone, and K. Chetty, "A survey on fundamental limits of integrated sensing and communication," *IEEE Commun. Surveys Tuts.*, vol. 24, no. 2, pp. 994–1034, 2nd Quart., 2022.
[9] D. K. P. Tan, J. He, Y. Li, A. Bayesteh, Y. Chen, P. Zhu, and W. Tong, "Integrated sensing and communication in 6G: Motivations, use cases, requirements, challenges and future directions," in *Proc. 1st IEEE Int. Online Symp. Joint Commun. Sens.*, Dresden, Germany, Feb. 2021, pp. 1–6.
[10] Z. Feng, Z. Fang, Z. Wei, X. Chen, Z. Quan, and D. Ji, "Joint radar and communication: A survey," *China Commun.*, vol. 17, no. 1, pp. 1–27, Jan. 2020.
[11] F. Liu, C. Masouros, A. P. Petropulu, H. Griffiths, and L. Hanzo, "Joint radar and communication design: Applications, state-of-the-art, and the road ahead," *IEEE Trans. Commun.*, vol. 68, no. 6, pp. 3834–3862, Jun. 2020.
[12] N. Bahadori, N. Namvar, B. Kelleyy, and A. Homaifar, "Device-to-device communications in millimeter wave band: Impact of beam alignment error," in *Proc. Wireless Telecommun. Symp. (WTS)*, Apr. 2019, pp. 1–6.
[13] F. Liu, W. Yuan, C. Masouros, and J. Yuan, "Radar-assisted predictive beamforming for vehicular links: Communication served by sensing," *IEEE Trans. Wireless Commun.*, vol. 19, no. 11, pp. 7704–7719, Nov. 2020.
[14] U. Demirhan and A. Alkhateeb, "Radar aided 6G beam prediction: Deep learning algorithms and real-world demonstration," in *Proc. IEEE Wireless Commun. Netw. Conf. (WCNC)*, Apr. 2022, pp. 2655–2660.
[15] A. Ali, N. Gonzlez-Prelcic, and A. Ghosh, "Millimeter wave V2I beam-training using base-station mounted radar," in *Proc. IEEE Radar Conf. (RadarConf)*, Apr. 2019, pp. 1–5.
[16] N. González-Prelcic, R. Méndez-Rial, and R. W. Heath, "Radar aided beam alignment in mmWave V2I communications supporting antenna diversity," in *Proc. Inf. Theory Appl. Workshop (ITA)*, Mar. 2016, pp. 1–7.
[17] G. R. Muns, K. V. Mishra, C. B. Guerra, Y. C. Eldar, and K. R. Chowdhury, "Beam alignment and tracking for autonomous vehicular communication using IEEE 802.11 ad-based radar," in *Proc. IEEE INFOCOM Conf. Comput. Commun. Workshops (INFOCOM WKSHPS)*, Apr. 2019, pp. 535–540.
[18] M. Rebato, J. Park, P. Popovski, E. De Carvalho, and M. Zorzi, "Stochastic geometric coverage analysis in mmWave cellular networks with realistic channel and antenna radiation models," *IEEE Trans. Commun.*, vol. 67, no. 5, pp. 3736–3752, May 2019.
[19] A. Al-Hourani, R. J. Evans, S. Kandeepan, B. Moran, and H. Eltom, "Stochastic geometry methods for modeling automotive radar interference," *IEEE Trans. Intell. Transp. Syst.*, vol. 19, no. 2, pp. 333–344, Feb. 2018.
[20] Z. Fang, Z. Wei, X. Chen, H. Wu, and Z. Feng, "Stochastic geometry for automotive radar interference with RCS characteristics," *IEEE Wireless Commun. Lett.*, vol. 9, no. 11, pp. 1817–1820, Nov. 2020.
[21] S. S. Ram, G. Singh, and G. Ghatak, "Estimating radar detection coverage probability of targets in a cluttered environment using stochastic geometry," in *Proc. IEEE Int. Radar Conf. (RADAR)*, Apr. 2020, pp. 665–670.
[22] S. S. Ram and G. Ghatak, "Estimation of bistatic radar detection performance under discrete clutter conditions using stochastic geometry," in *Proc. IEEE Radar Conf. (RadarConf22)*, Mar. 2022, pp. 1–6.
[23] S. S. Ram, G. Singh, and G. Ghatak, "Optimization of radar parameters for maximum detection probability under generalized discrete clutter conditions using stochastic geometry," *IEEE Open J. Signal Process.*, vol. 2, pp. 571–585, 2021.
[24] N. R. Olson, J. G. Andrews, and R. W. Heath, "Coverage and rate of joint communication and parameter estimation in wireless networks," *IEEE Trans. Inf. Theory*, vol. 70, no. 1, pp. 206–243, Jan. 2024.
[25] P. Ren, A. Munari, and M. Petrova, "Performance tradeoffs of joint radar-communication networks," *IEEE Wireless Commun. Lett.*, vol. 8, no. 1, pp. 165–168, Feb. 2019.
[26] Z. Fang, Z. Wei, Z. Feng, X. Chen, and Z. Guo, "Performance of joint radar and communication enabled cooperative detection," in *Proc. IEEE/CIC Int. Conf. Commun. China (ICCC)*, Aug. 2019, pp. 753–758.
[27] H. Ma, Z. Wei, X. Chen, Z. Fang, Y. Liu, F. Ning, and Z. Feng, "Performance analysis of joint radar and communication enabled vehicular ad hoc network," in *Proc. IEEE/CIC Int. Conf. Commun. China (ICCC)*, Aug. 2019, pp. 887–892.
[28] M. Kafafy, A. S. Ibrahim, and M. H. Ismail, "Stochastic geometry-based performance analysis of cellular systems in the vicinity of rotating radars," *IEEE Commun. Lett.*, vol. 25, no. 4, pp. 1391–1395, Apr. 2021.
[29] P. Ren, A. Munari, and M. Petrova, "Performance analysis of a time-sharing joint radar-communications network," in *Proc. Int. Conf. Comput., Netw. Commun. (ICNC)*, Feb. 2020, pp. 908–913.
[30] C. Skouroumounis, C. Psomas, and I. Krikidis, "FD-JCAS techniques for mmWave HetNets: Ginibre point process modeling and analysis," *IEEE Trans. Mobile Comput.*, vol. 21, no. 12, pp. 4352–4366, Dec. 2022.
[31] S. S. Ram, S. Singhal, and G. Ghatak, "Optimization of network throughput of joint radar communication system using stochastic geometry," *Frontiers Signal Process.*, vol. 2, p. 28, Apr. 2022.
[32] I. Tropkina, B. Sun, D. Moltchanov, A. Pyattaev, B. Tan, R. Dinis, and S. Andreev, "Distributed communication and sensing system co-design for improved UAV network resilience," *IEEE Trans. Veh. Technol.*, vol. 72, no. 1, pp. 924–939, Jan. 2023.
[33] X. Li, S. Guo, T. Li, X. Zou, and D. Li, "On the performance trade-off of distributed integrated sensing and communication networks," *IEEE Wireless Commun. Lett.*, vol. 12, no. 12, pp. 2033–2037, Dec. 2023.
[34] Y. Nabil, H. ElSawy, S. Al–Dharrab, H. Attia, and H. Mostafa, "A stochastic geometry analysis for joint radar communication system in millimeter-wave band," in *Proc. IEEE Int. Conf. Commun. (ICC)*, May 2023, pp. 5849–5854.
[35] D. K. John and J. M. Ronald, *Antennas: For All Applications*. New York, NY, USA: McGraw-Hill, 2002.
[36] N. R. Olson, J. G. Andrews, and R. W. Heath Jr., "Coverage and rate of joint communication and parameter estimation in wireless networks," 2022, *arXiv:2210.02289*.
[37] M. R. Akdeniz, Y. Liu, M. K. Samimi, S. Sun, S. Rangan, T. S. Rappaport, and E. Erkip, "Millimeter wave channel modeling and cellular capacity evaluation," *IEEE J. Sel. Areas Commun.*, vol. 32, no. 6, pp. 1164–1179, Jun. 2014.
[38] P. Swerling, "Probability of detection for fluctuating targets," *IRE Trans. Inf. Theory*, vol. IT-6, no. 2, pp. 269–308, Apr. 1960.
[39] M. Jankiraman, *FMCW Radar Design*. Norwood, MA, USA: Artech House, 2018.
[40] M. Sekine and Y. Mao, *Weibull Radar Clutter*, vol. 3. London, U.K.: IET, 1990.
[41] D. K. Barton, *Modern Radar System Analysis*. Norwood, MA, USA: Artech House, 1988.
[42] D. K. Barton, *Radar System Analysis and Modeling*. Norwood, MA, USA: Artech House, 2004.
[43] J. A. Zhang, M. L. Rahman, K. Wu, X. Huang, Y. J. Guo, S. Chen, and J. Yuan, "Enabling joint communication and radar sensing in mobile networks—A survey," *IEEE Commun. Surveys Tuts.*, vol. 24, no. 1, pp. 306–345, 1st Quart., 2021.
[44] M. Shi, K. Yang, C. Xing, and R. Fan, "Decoupled heterogeneous networks with millimeter wave small cells," *IEEE Trans. Wireless Commun.*, vol. 17, no. 9, pp. 5871–5884, Sep. 2018.
[45] H. Alzer, "On some inequalities for the incomplete gamma function," *Math. Comput.*, vol. 66, no. 218, pp. 771–778, 1997.

YASSER NABIL received the B.Sc. degree in electronics and communications engineering from Alexandria University, Alexandria, Egypt, in 2016, the Diploma degree in wireless communications from the Information Technology Institute, Ministry of Communications and Information Technology, Giza, Egypt, in 2020, and the M.Sc. degree in electronics and communications engineering from Cairo University, Giza, in 2023. He is currently pursuing the Ph.D. degree in electrical and computer engineering with Queen's University, Kingston, ON, Canada.

From 2020 to 2023, he was a Research Assistant with the One Laboratory, Egypt. His research interests include wireless communication systems and their statistical modeling, aerial communication, optical communication, and the integration of communication and sensing.

HESHAM ELSAWY (Senior Member, IEEE) received the Ph.D. degree in electrical engineering from the University of Manitoba, Canada, in 2014. He is currently an Assistant Professor with the School of Computing, Queen's University, Kingston, ON, Canada. Prior to that, he was an Assistant Professor with the King Fahd University of Petroleum and Minerals (KFUPM), Saudi Arabia, a Postdoctoral Fellow with the King Abdullah University of Science and Technology (KAUST), Saudi Arabia, a Research Assistant with TRTech, Winnipeg, MB, Canada, and a Telecommunication Engineer with the National Telecommunication Institute, Egypt. He is a recipient of the IEEE ComSoc Outstanding Young Researcher Award for Europe, Middle East & Africa Region, in 2018. He also received several best paper awards, including the IEEE COMSOC Best Tutorial Paper Award, in 2020, and IEEE COMSOC Best Survey Paper Award, in 2017. He is an Editor of IEEE TRANSACTIONS ON WIRELESS COMMUNICATIONS, IEEE COMMUNICATIONS SURVEYS AND TUTORIALS, and IEEE COMMUNICATIONS LETTERS. He is recognized as an Exemplary Editor of IEEE COMMUNICATIONS LETTERS and an Exemplary Reviewer of IEEE TRANSACTIONS ON COMMUNICATIONS, IEEE TRANSACTIONS ON WIRELESS COMMUNICATIONS, and IEEE WIRELESS COMMUNICATIONS LETTERS. He conducts research in the broad area of wireless communications and networking with a special focus on 5G/6G networks, the Internet of Things, edge computing, and non-terrestrial networks.

SUHAIL AL-DHARRAB (Senior Member, IEEE) received the B.Sc. degree in electrical engineering from the King Fahd University of Petroleum and Minerals (KFUPM), Dhahran, Saudi Arabia, in 2005, and the M.A.Sc. and Ph.D. degrees in electrical and computer engineering from the University of Waterloo, Waterloo, ON, Canada, in 2009 and 2013, respectively. From 2005 to 2007, he was a Graduate Assistant with the Electrical Engineering Department, KFUPM. In 2015, he was a Visiting Professor with the School of Electrical and Computer Engineering, Georgia Institute of Technology, Atlanta, USA. He is currently an Assistant Professor with the Electrical Engineering Department, an Affiliate with the Interdisciplinary Research Center for Communication Systems and Sensing, and the Assistant Dean of Research with KFUPM. His research interests include the areas of wireless communication systems, underwater acoustic communication, digital signal processing, and information theory.

HASSAN MOSTAFA (Senior Member, IEEE) received the B.Sc. and M.Sc. degrees (Hons.) in electronics engineering from Cairo University, Cairo, Egypt, in 2001 and 2005, respectively, and the Ph.D. degree in electrical and computer engineering from the Department of Electrical and Computer Engineering, University of Waterloo, Waterloo, ON, Canada, in 2011.

He is currently an Associate Professor with the Nanotechnology and Nano-Electronics Program, Zewail City of Science and Technology, Egypt, on leave from the Department of Electronics and Electrical Communications, Cairo University. He was an NSERC Postdoctoral Fellow with the Department of Electrical and Computer Engineering, University of Toronto, Toronto, ON. His postdoctoral work includes the design of the next generation FPGA in collaboration with Fujitsu Research Labs, Japan/USA. He has authored/coauthored over 250 papers in international journals and conferences and he is the author/coauthor of five published books. His research interests include neuro-morphic computing, the IoT hardware security, software defined radio, reconfigurable low power systems, analog-to-digital converters (ADCs), low-power circuits, sub-threshold logic, variation-tolerant design, soft error tolerant design, statistical design methodologies, next generation FPGA, spintronics, memristors, energy harvesting, MEMS/NEMS, power management, and opto-electronics.

Dr. Mostafa has been a member of the IEEE Technical Committee of VLSI Systems and Applications (TC-VSA), since 2017. In addition, he was an associate editor and a guest editor of several journals and also he has been the conference technical chair and the track chair of various conferences, since 2015. He was a recipient of the University of Toronto Research Associate Scholarship, in 2012, the Natural Sciences and Engineering Research Council of Canada (NSERC) Prestigious Postdoctoral Fellowship, in 2011, the Waterloo Institute of Nano-technology (WIN) Nano-Fellowship Research Excellence Award, in 2010, the Ontario Graduate Scholarship (OGS), in 2009, and the University of Waterloo SandFord Fleming TA Excellence Award, in 2008.

HUSSEIN ATTIA (Member, IEEE) received the Ph.D. degree in electrical and computer engineering from the University of Waterloo, Waterloo, ON, Canada, in 2011. He was a Research Engineer with the Coding and Signal Transmission Laboratory, University of Waterloo, from March 2011 to July 2013. He was granted a Postdoctoral Fellowship with Concordia University, Montreal, QC, Canada, from August 2014 to July 2015. Also, he was a Visiting Scholar with Quebec University (INRS), from August 2015 to December 2015 and from June 2017 to August 2017. He is currently an Associate Professor and the Director of the Applied Electromagnetics Laboratory, King Fahd University of Petroleum and Minerals (KFUPM). He is also an Associate Editor of IEEE ANTENNAS AND WIRELESS PROPAGATION LETTERS and IEEE ACCESS. He has published about 100 journals and conference papers. His research interests include applied electromagnetics, biomedical engineering, microwave sensors, millimeter-wave antennas, analytical techniques for electromagnetic modeling, and metamaterials. He received several awards, including a full Ph.D. scholarship from the Ministry of Higher Education, Egypt, from 2007 to 2011, the University of Waterloo Graduate Scholarship for excellence in research and coursework, in 2009, and a certificate in University Teaching from the University of Waterloo, in 2010. He was a Finalist in the Best Paper Competition of the 2011 IEEE AP-S International Symposium on Antennas and Propagation. He ranked first among all B.Sc. electronics and communication engineering students with Zagazig University, Egypt, in 1999.